Compressional behavior of solid $NeHe_2$ up to 90 GPa

2010 J. Phys.: Condens. Matter 22 095401

(http://iopscience.iop.org/0953-8984/22/9/095401)

J. Phys.: Condens. Matter **22** (2010) 095401 (8pp) doi:10.1088/0953-8984/22/9/095401

Compressional behavior of solid $NeHe_2$ up to 90 GPa

Hiroshi Fukui[1,3], **Naohisa Hirao**[2], **Yasuo Ohishi**[2] and **Alfred Q R Baron**[1,2]

[1] Materials Dynamics Laboratory, RIKEN, Kouto 1-1-1, Sayo, Hyogo 679-5148, Japan
[2] Japan Synchrotron Radiation Research Institute, SPring-8, Kouto 1-1-1, Sayo, Hyogo 679-5148, Japan

E-mail: fukuih@spring8.or.jp

Received 28 September 2009, in final form 21 January 2010
Published 10 February 2010
Online at stacks.iop.org/JPhysCM/22/095401

Abstract

$NeHe_2$ was compressed to about 90 GPa using a diamond anvil cell technique. The crystal structure was confirmed to be stable with hexagonal symmetry in the investigated pressure range and its p–V equation of state was determined by angular dispersive x-ray diffraction with synchrotron radiation. With the help of *ab initio* calculations, the compressibility and inter-atomic distances of $NeHe_2$ were compared with those of a helium and neon mixture of the same composition. This study shows that the bulk modulus of $NeHe_2$ is between those of neon and helium and that linear compressibilities of the inter-atomic distances are different from those of the elementary solids. This material can be a pressure-transmitting medium, providing both a large sample space and good quasi-hydrostatic conditions.

(Some figures in this article are in colour only in the electronic version)

1. Introduction

The properties of condensed gases at high pressure attracts a great deal of experimental and theoretical attention since these materials provide critical tests of the theories of bonding in solids. In particular, rare-gas solids are an important class of materials for chemical physics since they have long been considered a prototype for understanding van der Waals (vdW) interactions. Considerable effort has been expended to determine the inter-atomic potentials for rare-gas solids, including the possible effects of many-body forces (e.g. [1–3]). Experimental data about the physical properties of the noble-gas solids are desirable for a quantitative understanding of the potentials. Their high pressure structural and elastic properties are important for the Earth and planetary sciences, especially the interior of the giant gas planets such as Jupiter. These materials also have a significant role as pressure-transmitting media in high pressure experiments using diamond anvil cells: helium, neon and argon are often used as pressure-transmitting media due to, for example, the softness, transparency, chemical inertness and simplicity of the crystal structures related to the number of x-ray diffraction lines.

We focus on the high pressure behavior of helium and neon mixtures. Loubeyre *et al* (1987) determined the binary phase diagram of He–Ne, finding a stoichiometric compound is formed at 12.8 GPa, and measured its volume at 13.7 and 21.8 GPa [4]. This substance belongs to the $P6_3/mmc$ space group, where helium occupy 2a (He1) and 6h (He2) sites and neon 4f sites. This structure is known as an $MgZn_2$-type hexagonal Laves phase structure [5], where neon atoms form a hexagonal diamond sublattice and helium atoms are in the sublattice and form triangular bipyramidal chains (see figure 1)[4]. The stability and the compressional behavior of the Laves-$NeHe_2$ have not been reported at higher pressures. We have performed x-ray diffraction measurements on the $NeHe_2$ system under high pressure conditions to determine its crystal structure and p–V equation of state up to 90 GPa. We compared the measured compressional behavior with calculations of a hypothetical helium and neon mixture. We also evaluated this mixture as a pressure-transmitting medium.

2. Experimental procedure

X-ray diffraction experiments were carried out using a diamond anvil cell in an angle-dispersive mode at BL04B2 of

[3] Author to whom any correspondence should be addressed. Present address: Graduate School of Material Science, University of Hyogo, 3-2-1, Kamigohri, Hyogo 678-1279, Japan.

[4] This figure was drawn by VESTA. See [6] about this application.

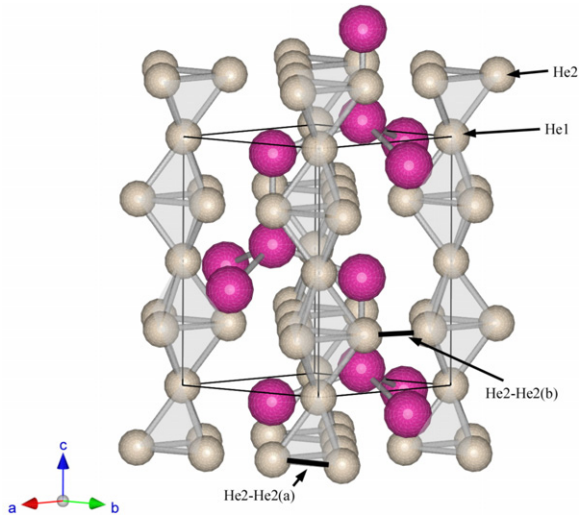

Figure 1. Crystal structure of the Laves-$NeHe_2$ drawn with atomic coordinate parameters of $MgZn_2$ [5]. Light and dark pink balls are helium and neon atoms, respectively. Thin lines indicate the unit cell. The space group is $P6_3/mmc$, where helium occupies 2a (He1) and 6h (He2) sites and neon occupies 4f sites. Neon atoms form a hexagonal diamond sublattice. Five helium atoms (two He1 and three He2) make triangular bipyramids which link along the c axis by He1. The chains are connected to each other by He2–He2(b) bonds, which are not drawn in the figure.

SPring-8 [7]. The incident beam was collimated with a 40 μm pinhole. The diffraction patterns were recorded on an image plate and the set-up was calibrated using CeO_2 powder as a standard. A two-dimensional image from the imaging plate was processed and analyzed by pattern-integration software, PIP [8]. We performed two experimental runs with different DACs, depending on the experimental pressure ranges. The calibrated wavelength of the incident x-ray was 0.329 23 and 0.330 95 Å for Runs 1 and 2, respectively. Diamond anvils, with a no-beveled 350 μm diameter culet (Run 1), and a 150 μm diameter anvil face and a 10° bevel angle (Run 2), were used for generating pressure. A rhenium metal gasket with a 160 μm diameter hole and initial thickness of 50 μm (Run 1) and a 110 μm hole and initial thickness of 35 μm (Run 2) was used to contain a starting sample that was a compressed gas mixture of neon and helium in 1:2 ratios up to 190 MPa. The diameter of the sample chamber typically decreased to 103 μm at approx. 7 GPa and 74 μm at approx. 21 GPa in Runs 1 and 2, respectively. We loaded gold powder (∼99.99% pure and 8 μm diameter) and a few ruby balls or chips (5–15 μm in size) with the sample as pressure standard materials. The initial occupancies of gold and ruby in the sample chamber of Run 1 were estimated from a visible image and were 2.6 and 2.9% in volume, respectively. The DACs were fixed on the diffractometer and not oscillated during exposures. The ruby R lines were excited with an Ar-ion laser before and after x-ray exposure. The experimental pressure was estimated from the unit cell volume of gold using the reported equation of state [9]. The ruby fluorescence provided an additional check on the pressure in the sample chamber [10]. All measurements were performed at 300 K.

3. Calculations

In order to estimate the internal atomic coordinates of the Laves-$NeHe_2$, we have performed first principal calculations under the *ab initio* full potential density functional theory (DFT) with the augmented plane wave (APW) method using the program package WIEN2k [11]. Indeed, advanced attempts are probably required in order to implement the vdW interaction in DFT (e.g. [12, 13]). However, without taking special terms for vdW into account, a rather conventional DFT calculation, using the local density (LDA) or generalized gradient (GGA) approximations, can yield short-range interactions and mechanical properties of vdW solids [14]. We therefore consider that the conventional DFT calculation helps us to understand the behavior of $NeHe_2$. In this study, exchange and correlation effects were accounted for by the GGA. The atomic radii were set as 1.80 au for helium and 2.13 au for neon. An energy cutoff to separate core from valence states was chosen as −6.0 Ryd. RKmax (related to the plane wave cutoff) and Gmax (related to the charge cutoff) were 7 and 14, respectively. The optimizations of the atomic positions with fixed lattice constants from the experimental observations were performed with 100 k-points until the forces between atoms became less than 1.0 mRy au^{-1}. At the end of the self-consistent field (scf) iterations the total energy difference between iterations and the charge distance was less than 0.0002 Ryd and 0.0005e, respectively, in all calculations. Several sets of initial values of atomic coordinates were used to confirm the results independent of the input atomic coordinates.

4. Results and discussion

The measured pressure points are listed in table 1. Diffraction from the sample of $NeHe_2$ was not observed below 15 GPa although the reported solidifying pressure was 12.8 GPa [4]. This is most probably because $NeHe_2$ crystallized into relatively large grains which could not be detected without any oscillation of the DAC. Figure 2 shows typical diffraction patterns recorded in these experiments. The sample was pressurized quickly in Run 2 to promote nucleation and therefore the grain growth was limited and a polycrystalline structure was realized under pressure. The diffraction pattern of Run 1 showed spots from the sample, indicating relatively large grains existed, whereas they appeared as streaks in the diffraction pattern of Run 2, meaning the sample was more powder-like than that in Run 1. The reflections were sharp at lower pressures and showed symmetric broadening as the pressure was increased. All diffraction patterns obtained in the pressure range of this experiment were indexed with gold, rhenium and a hexagonal lattice. The number of observed diffraction lines belonging to the hexagonal lattice was 12 in most cases. Since the intensity of the diffraction lines was weak at high diffraction angles, the lines were not obstacles to the determination of the diffraction peak positions of gold. No indication of pure helium or neon was observed. This means that the reported Laves phase of $NeHe_2$ is stable up to at least 85 GPa at room temperature conditions. The transparency to visible light was kept in the whole pressure region examined.

Table 1. Lattice parameters of gold and $NeHe_2$ under high pressure conditions. Parameters of M_0 and M_1 for gold (see text) and obtained cell parameters and unit cell volumes of $NeHe_2$ are also listed. Standard deviations of the lattice parameter of gold obtained in the fitting procedure are shown in parentheses. The values in parentheses for pressure are estimated errors in the case that the error source should be the standard deviations of the lattice parameters of gold only.

		Gold			$NeHe_2$		
Run	p (GPa)	a (Å)	M_0	M_1	a (Å)	c (Å)	V (Å^3)
1	7.445 96(2)	4.0251(3)	4.0256	−0.4	—	—	—
	10.441(1)	4.0068(2)	4.0075	−0.5	—	—	—
	10.331(3)	4.0074(3)	4.0082	−0.6	—	—	—
	15.106 0(4)	3.9808(1)	3.9811	−0.5	—	—	—
	17.902 9(2)	3.9665(2)	3.9666	−0.4	4.020(2)	6.475(22)	90.61(32)
	19.611(2)	3.9582(2)	3.9582	−0.3	3.977(1)	6.450(2)	88.36(4)
	19.729(4)	3.9576(3)	3.9582	−0.5	3.924(2)	6.375(6)	85.01(11)
	25.97(1)	3.9295(5)	3.9309	−2.0	3.843(1)	6.116(3)	78.22(4)
	27.98(3)	3.9211(7)	3.9228	−3.4	3.804(3)	6.041(12)	75.69(20)
	33.98(3)	3.8976(6)	3.9000	−4.1	3.748(2)	5.964(10)	72.55(15)
	36.43(4)	3.8886(7)	3.8900	−3.2	3.712(4)	5.978(18)	71.33(28)
	39.74(14)	3.8769(13)	3.8784	−2.6	3.683(3)	5.939(12)	69.78(18)
	43.34(3)	3.8648(6)	3.8669	−3.5	3.657(2)	5.953(8)	68.93(12)
	46.11(8)	3.8559(9)	3.8564	−2.1	3.638(1)	5.935(6)	68.04(9)
	47.99(5)	3.8500(7)	3.8512	−3.1	3.624(4)	5.838(15)	66.41(22)
	50.94(16)	3.8410(12)	3.8424	−3.7	3.603(1)	5.904(4)	66.37(6)
	53.55(23)	3.8334(14)	3.8341	−2.8	3.583(2)	5.903(9)	65.62(13)
	55.90(15)	3.8266(11)	3.8279	−3.7	3.568(3)	5.884(13)	64.87(19)
	56.89(33)	3.8238(16)	3.8237	−2.9	3.549(2)	5.887(4)	64.23(8)
2	24.010(2)	3.9380(2)	3.9391	−2.0	3.852(1)	6.272(2)	80.59(5)
	26.483(5)	3.9273(3)	3.9296	−3.5	3.815(5)	6.231(8)	78.55(23)
	30.66(2)	3.9103(6)	3.9130	−3.0	3.770(2)	6.155(4)	75.77(10)
	34.55(1)	3.8954(4)	3.8972	−2.3	3.732(2)	6.114(3)	73.73(10)
	39.029(8)	3.8794(3)	3.8808	−1.8	3.683(3)	6.026(4)	70.81(11)
	43.459(4)	3.8644(2)	3.8661	−2.4	3.647(5)	5.982(8)	68.89(20)
	45.23(2)	3.8587(5)	3.8604	−2.7	3.630(6)	5.949(10)	67.88(24)
	51.31(2)	3.8340(4)	3.8420	−3.0	3.574(6)	5.911(6)	65.37(22)
	53.53(2)	3.8334(4)	3.8355	−2.9	3.553(6)	5.896(9)	64.46(24)
	58.59(8)	3.8191(8)	3.8221	−3.4	3.528(7)	5.829(17)	62.83(31)
	61.37(20)	3.8116(12)	3.8151	−3.9	3.537(9)	5.773(27)	62.55(42)
	64.23(7)	3.8041(7)	3.8067	−3.2	3.524(10)	5.742(28)	61.75(46)
	68.64(3)	3.7929(4)	3.7942	−1.9	3.498(4)	5.735(11)	60.76(17)
	71.01(3)	3.7871(4)	3.7876	−2.9	3.471(4)	5.699(16)	59.46(22)
	72.27(9)	3.7840(7)	3.7880	−1.5	3.466(4)	5.683(15)	5912(21)
	75.02(7)	3.7775(6)	3.7792	−2.7	3.450(4)	5.657(14)	58.31(19)
	76.93(2)	3.7731(3)	3.7752	−3.2	3.439(3)	5.644(11)	57.81(14)
	80.24(13)	3.7656(8)	3.7677	−3.2	3.442(7)	5.610(14)	57.57(27)
	82.17(53)	3.7613(16)	3.7647	−4.0	3.415(8)	5.590(23)	56.47(35)
	82.67(7)	3.7602(6)	3.7615	−3.7	3.416(2)	5.615(4)	56.75(8)
	83.68(3)	3.7580(4)	3.7602	−4.0	3.419(3)	5.614(5)	56.82(11)
	85.51(2)	3.7540(3)	3.7563	−3.8	3.411(3)	5.608(5)	56.51(10)

4.1. Equation of state and inter-atomic distances

The obtained unit cell volumes from the hexagonal indexed diffraction peaks are plotted against pressure with the previous results in figure 3(a). From this plot, the bulk modulus can be obtained by fitting these data to a universal equation of state $P = 3K_{T0}\frac{1-(\frac{V}{V_0})^{1/3}}{(\frac{V}{V_0})^{2/3}}\exp[\frac{3(K'_{T0}-1)}{2}\{1-(\frac{V}{V_0})^{1/3}\}]$ [15], where K_{T0}, K'_{T0} and V_0 are bulk modulus, its pressure derivative and a unit cell volume at zero pressure, respectively. The determined compressional curve drawn in figure 3 shows good agreement with the experimental data points, yielding $K_{T0} = 5.7 \pm 8.2$ GPa, $K'_{T0} = 5.8 \pm 1.4$ and $V_0 = 160 \pm 43$ Å^3. The large error is probably due to the lack of data points below 15 GPa. In the analysis with fixed V_0, we obtained $K_{T0} = 1.7 \pm 0.1$ and $K'_{T0} = 6.9 \pm 0.1$ with 203 Å^3, and $K_{T0} = 31.6 \pm 1.3$ $K'_{T0} = 3.9 \pm 0.1$ with 117 Å^3. The difference between volumes calculated with these three parameter sets is less than 1% above 25 GPa. The compression curve shows excellent agreement with the literature values [4].

We have compared the elastic property of the Laves-$NeHe_2$ presently obtained with that of a hypothetical helium–neon mixture calculated with the EoSs of helium [16] and neon [17, 18]. Note that the reported EoS of helium [16] reproduces observed volumes up to 60 GPa [19] although the EoS was determined with data up to 32 GPa. Volumes with the 4Ne–8He mixture are compared in figure 3(a) since there are four formula units in the unit cell of the Laves-$NeHe_2$. The volumes of $NeHe_2$ were smaller than those of the mixture at pressure conditions below 30 GPa. The volumes of $NeHe_2$ are

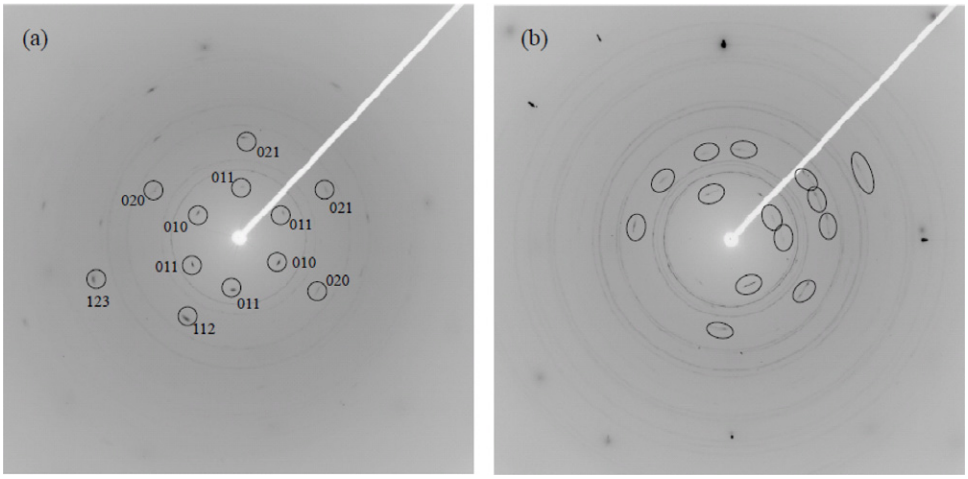

Figure 2. 2D diffraction patterns obtained in Run 1 at 46.1 GPa (a) and Run 2 at 45.2 GPa (b). Representative diffraction signals from $NeHe_2$ are indicated by circles. The Miller indices of the Laves-$NeHe_2$ are displayed in (a). Their intensities were stronger in Run 1 than those in Run 2 since the size of the sample chamber was different. In the pattern of Run 2, diffraction from the rhenium gasket is also seen.

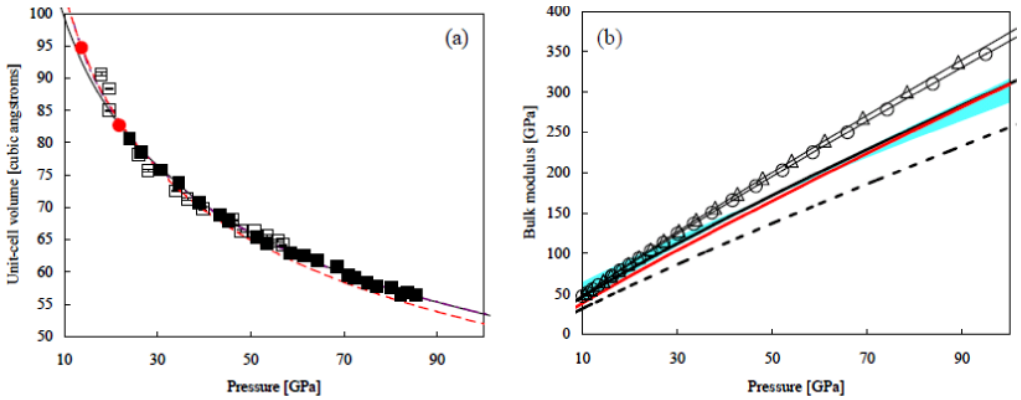

Figure 3. (a) Pressure dependence of the unit volume of $NeHe_2$ at 300 K. Open and solid squares are experimentally obtained values in Run 1 and Run 2, respectively. The solid line is the fitted compression curve to Vinet's equation. Red circles are literature values [4]. A red broken line shows the volume of a mixture of 4Ne and 8He from [16] and [17]. (b) Pressure dependence of bulk moduli of $NeHe_2$ (thick solid curve), Ne (thin solid curves with symbols: triangles for [17] and circles for [18]), He (dotted curve from [19]) and the neon–helium mixture (red curve calculated with parameters of [16, 17]) at 300 K. A light blue area indicates upper and lower bounds of the bulk modulus obtained with the two parameter sets.

almost the same or slightly larger than those of the mixture above this pressure. The difference in the volume between the Laves-$NeHe_2$ and the mixture does not change so much above 100 GPa, indicating that the free energy of this system is unlikely to decrease drastically by decomposition of the Laves-$NeHe_2$.

We have also compared bulk moduli by differentiating the EoS. The pressure variation of bulk moduli is shown in figure 3(b) together with those of helium and neon. The averaged bulk modulus of the mixture was calculated by Voigt's method. The bulk modulus of the Laves-$NeHe_2$ is larger than that of the mixture at low pressures. Since the Voigt average generally gives the upper limit, the Laves-$NeHe_2$ has a larger bulk modulus than the mixture below 50 GPa, even taking the uncertainty in the bulk modulus, which originates from that of V_0 (see the foregoing discussion), into account. At around 10 GPa, the bulk modulus of $NeHe_2$ is comparable to that of neon. With increasing pressure, $NeHe_2$ has an intermediate value between helium and neon. Consequently, $NeHe_2$ at the initial compression is expected to have a smaller volume decrease than helium and to be softer than neon at high pressure. We will discuss this issue in the pressure variation of the bulk modulus with inter-atomic distances later.

The inter-atomic distances of the Laves-$NeHe_2$ with the measured lattice constants in Run 2 and literature values at 13.7 GPa [5] were obtained from the APW-DFT calculations. Since the Laves-$NeHe_2$ belongs to $P6_3/mmc$, the independent atomic coordinates are z(Ne) and x(He). The calculated atomic coordinates are shown in table 2. The average distance of each atomic pair is shown in figure 4(a). It was found that the Ne–He distance is longer than the mean of the Ne–Ne and He–He distances at all conditions, meaning that the bond strength between neon and helium may be weaker than that between the same kind of atoms. This microscopic structure is consistent with the bulk modulus of the Laves-$NeHe_2$ and is comparable to that of neon in the low pressure region. A dominant

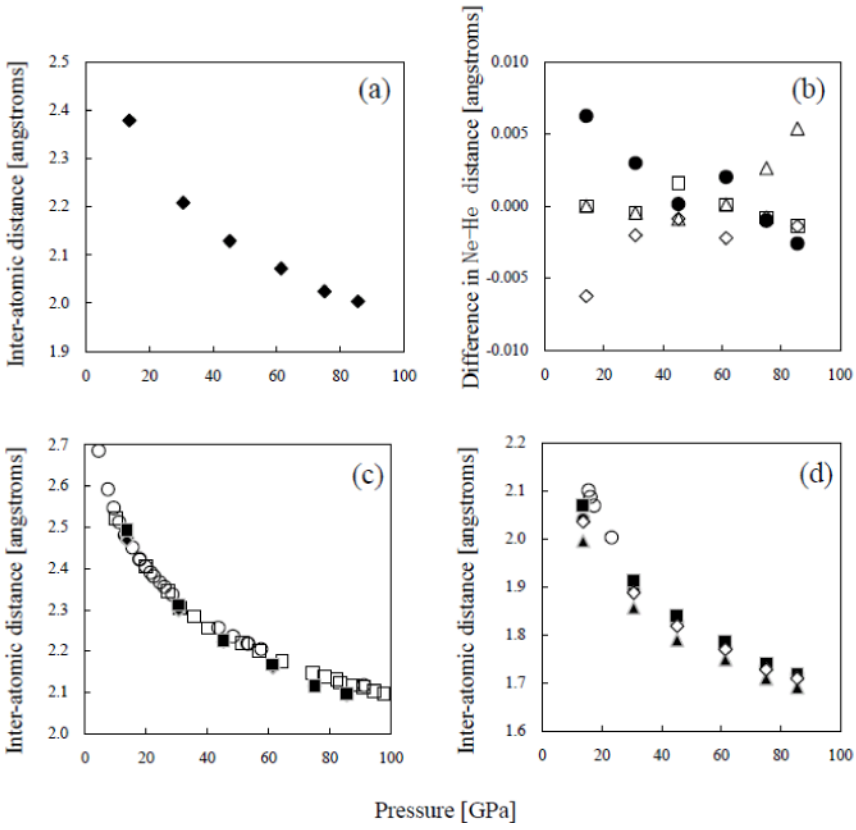

Figure 4. Pressure variation of inter-atomic distances. Present results of (a) average He–Ne distances and (b) difference from the average Ne–He1 (solid circles) and Ne–He2 (open diamonds, squares and triangles). (c) Present result of Ne–Ne distances (solid symbols) compared with those of [17] (open squares) and [18] (open circles). There are two different Ne–Ne distances. The shorter one, longer one and their weighed mean values are shown by solid diamonds, squares and circles, respectively. (d) Present results of He–He distances compared with those of [19] (open circles). There are three types of He–He pair, He1–He2, He2–He2(a) and He2–He2(b), indicated by solid circles, squares and triangles, respectively. Open diamonds indicate their weighed mean value. Error bars derived from the lattice constant determination are contained within the symbols.

compression mechanism in the low pressure region is probably the shortening of the Ne–Ne (and also Ne–He) distance. In order to compare the inter-atomic distances with those of the elemental substances, the inter-atomic distances of helium and neon were obtained from their lattice constants [17, 18, 20], since helium and neon occupy special positions, the 2c site of $P6_3/mmc$ and 4a site of $Fm\bar{3}m$, respectively. Ne–Ne distances are compared in figure 4(c), showing that there is no large difference between pure neon and the Laves-$NeHe_2$ below 30 GPa whereas that in the Laves-$NeHe_2$ is very slightly shorter than that in neon above 30 GPa. On the He–He distance shown in figure 4(d), those in the Laves-$NeHe_2$ are shorter than those in helium for all pressure ranges in the literature [20] and the difference seems to decrease with compression although there is no data point about helium at higher pressure. The inter-atomic distances in the Laves-$NeHe_2$ were found not to be compressed uniformly. At 30 GPa, the nearest inter-atomic distances were 92.8% of that at 14 GPa. However, the distances of Ne–Ne and Ne–He at 85.5 GPa were 84.2% of that at 14 GPa whereas that of He–He was 84.0%. In particular, the He2–He2(a) distance, which is the side of the bipyramid in the a–b plane, became 83%. However, the He2–He2(b), which is the distance between the bipyramidal chains, was 84.8%. From these points, the compression mechanism of the Laves-$NeHe_2$ in the high pressure region is a volume decrease of the triangular bipyramids of helium. The difference in the compression mechanism has probably appeared in the pressure variation of the bulk modulus, meaning that $NeHe_2$ tends to have a similar value to that of neon at lower pressures and intermediate ones between those of neon and helium at higher pressures. This compression behavior probably indicates the repulsion between different noble-gas atoms, which may be important in understanding the physical properties of noble-gas compounds.

4.2. Deviatoric stress conditions

For the cubic system, a direct way to evaluate the uniaxial stress component is to measure the d spacings of the sample by using the powder x-ray diffraction technique, and to analyze the systematic variation of the lattice parameter depending on the hkl indices [21]. We tried to estimate the deviatoric stress gold felt surrounded by $NeHe_2$ with this method. Using the notation by Takemura and Singh [22], the measured lattice parameter from a diffraction line with a Miller index of hkl, $a_m(hkl)$, is given by

$$a_m(hkl) = M_0 + M_1[3(1 - 3\sin^2\theta)\Gamma(hkl)], \qquad (1)$$

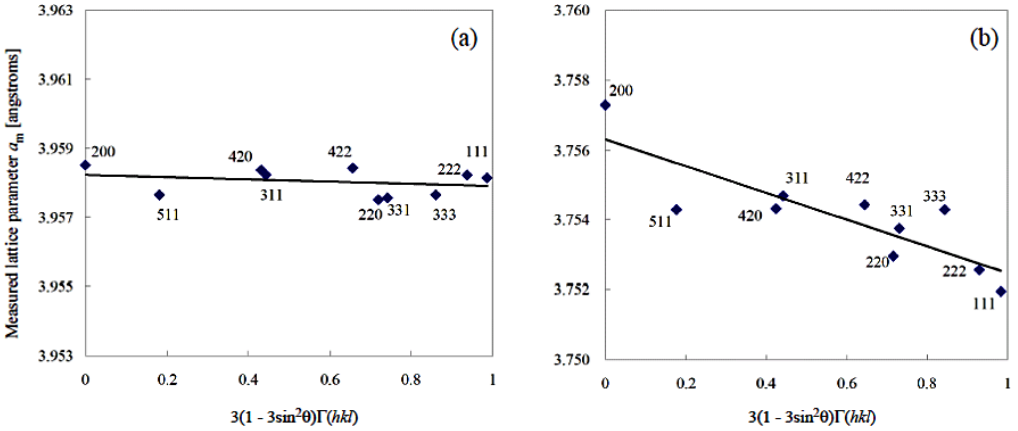

Figure 5. Representative gamma plots (a) 19.5 GPa in Run 1 and (b) 85.5 GPa in Run 2. Numbers in the plot indicate the Miller indices.

Table 2. Calculated atomic coordinates of the Laves-$NeHe_2$ and inter-atomic distances.

Pressure (GPa)	z(Ne)	x(He)	Ne–Ne	No. of bond	He–He	No. of bonds (type)	Ne–He	No. of bonds (type)
13.7	0.0634	0.3394	2.4687	1	2.0407	2(He1–He2)	2.3847	3(Ne–He1)
			2.4930	3	1.9955	2(He2–He2)	2.3722	3(Ne–He2)
					2.0705	2(He2–He2)	2.3785	6(Ne–He2)
			2.4869	Ave.	2.0356	Ave.	2.3785	Ave.
30.7	0.0633	0.3383	2.2985	1	1.8942	2(He1–He2)	2.2113	3(Ne–He1)
			2.3119	3	1.8570	2(He2–He2)	2.2063	3(Ne–He2)
					1.9132	2(He2–He2)	2.2079	6(Ne–He2)
			2.3086	Ave.	1.8881	Ave.	2.2083	Ave.
45.2	0.0632	0.3379	2.2224	1	1.8276	2(He1–He2)	2.1292	3(Ne–He1)
			2.2265	3	1.7902	2(He2–He2)	2.1282	3(Ne–He2)
					1.8397	2(He2–He2)	2.1307	6(Ne–He2)
			2.2255	Ave.	1.8192	Ave.	2.1291	Ave.
61.4	0.0629	0.3369	2.1600	1	1.7743	2(He1–He2)	2.0741	3(Ne–He1)
			2.1675	3	1.7495	2(He2–He2)	2.0699	3(Ne–He2)
					1.7874	2(He2–He2)	2.0722	6(Ne–He2)
			2.1656	Ave.	1.7704	Ave.	2.0721	Ave.
75.0	0.0630	0.3363	2.1162	1	1.7349	2(He1–He2)	2.0234	3(Ne–He1)
			2.1154	3	1.7095	2(He2–He2)	2.0236	3(Ne–He2)
					1.7404	2(He2–He2)	2.0237	3(Ne–He2)
							2.0271	3(Ne–He2)
			2.1156	Ave.	1.7283	Ave.	2.0245	Ave.
85.5	0.0630	0.3360	2.0970	1	1.7178	2(He1–He2)	2.0009	3(Ne–He1)
			2.0925	3	1.6920	2(He2–He2)	2.0021	6(Ne–He2)
					1.7193	2(He2–He2)	2.0089	3(Ne–He2)
			2.0936	Ave.	1.7097	Ave.	2.0035	Ave.

where

$$M_0 = a_p\left\{1 + \left(\frac{\alpha t}{3}\right)(1 - 3\sin^2\theta)[S_{11} - S_{12} - (1 - \alpha^{-1})(2G_V)^{-1}]\right\}, \quad (2a)$$

$$M_1 = -\frac{a_p \alpha t S}{3}, \quad (2b)$$

$$\Gamma(hkl) = (h^2k^2 + k^2l^2 + l^2h^2)/(h^2 + k^2 + l^2)^2, \quad (2c)$$

$$S = S_{11} - S_{12} - S_{44}/2. \quad (2d)$$

Here a_p is the lattice parameter under hydrostatic pressure, θ is half of the scattering angle, t is the uniaxial stress component or differential stress, which is positive if the axial stress component is larger than the in-plane stress component, S_{ij} denotes the single-crystal elastic compliance and G_V is the shear modulus of the polycrystalline aggregate under the assumption of strain continuity across the boundaries separating the crystallites. The parameter α determines the actual stress of the sample that is assumed to lie between the two extreme conditions of stress and strain continuity, and takes a value between 0.5 and 1. Figure 5 shows representative plots of $a_m(hkl)$ against $3(1 - 3\sin^2\theta)\Gamma(hkl)$, termed the gamma plot, for gold in the pressure medium of $NeHe_2$. The M_0 and M_1 can be obtained from this kind of plot with equation (1). The derivative of the plot, M_1, is almost zero at conditions even higher than the solidified pressure of $NeHe_2$, indicating that there is little effect of differential stress on gold diffraction data. With increasing pressure, the slope becomes steeper in a negative direction. The uniaxial stress t can

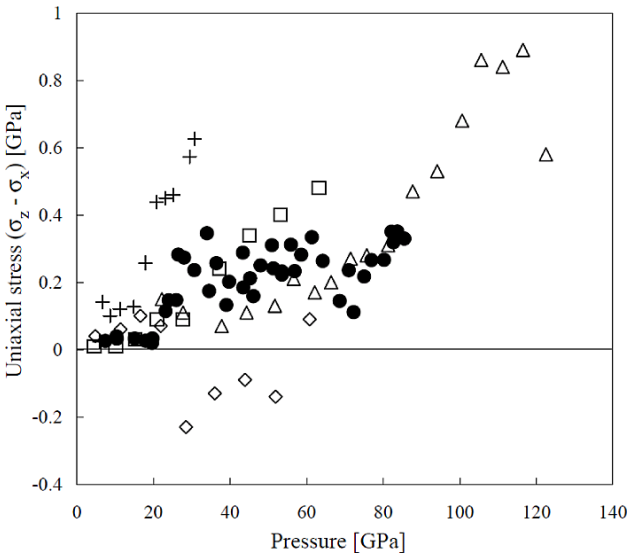

Figure 6. Estimated deviatoric stress in $NeHe_2$ from the gamma plots for gold (solid circles). The values of helium [23] (open symbols) and neon [25] (crosses) are also plotted for comparison.

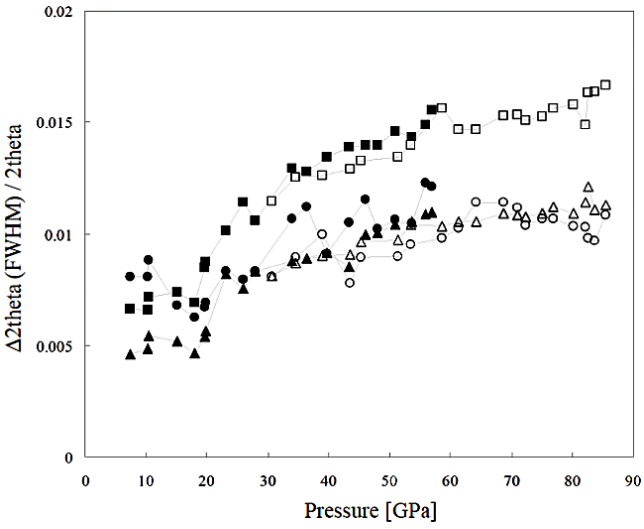

Figure 7. Pressure variation of x-ray diffraction linewidth normalized by the diffraction angle. Circles, squares and triangles indicate 111, 200, and 220 lines, respectively. Solid and open symbols correspond to Run 1 and Run 2, respectively.

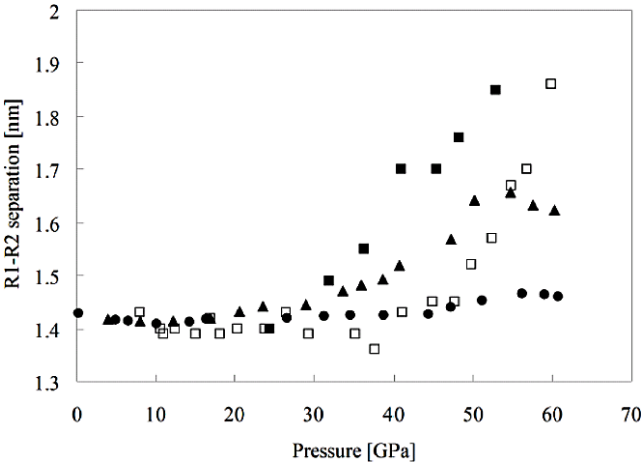

Figure 8. Pressure variation of separation of ruby fluorescence lines measured in Run 1 (open squares) and in Run 2 (solid squares) from the ambient pressure to 62 GPa. Those of helium and neon [26] are also shown for comparison by solid circles and triangles, respectively.

be estimated from $-3M_1/\alpha SM_0$ according to equations (2*b*) on assuming that $M_0 \sim a_p$ [23]. If the values of α and S are independent of the pressure medium, we obtained the relationship between t and M_1/M_0 from literature values [23]. Using the obtained relationship, we calculated deviatoric stress from M_1/M_0. The estimated uniaxial stress $t\,(=-3M_1/\alpha SM_0)$ is shown in figure 6. It should be noted that the values shown here are lower bounds of t since α is regarded as unity [23]. A positive value of t means that the stress component of the compressional axis was becoming larger than the other two axes in the plane perpendicular to the compressional axis. The deviation is significant at pressure conditions over 20 GPa.

The stress condition is also evaluated from the full width at half-maximum (FWHM) of diffraction peaks. Here, the FWHM of the 111, 200, and 220 lines were plotted since the peak fitting of these three lines is better than the others due to their large intensity. In particular of Run 2, peaks of gold usually overlapped with those from the rhenium gasket since the incident beam size was not small enough. Figure 7 shows the FWHM normalized with the diffraction angle 2θ as a function of pressure. The width of these three lines gradually increased with increasing pressure, which is consistent with the previous study using gold powder in a helium medium [23]. It is notable that the linewidth of Au 200 and 220 increased between 20 and 26 GPa whereas that of Au 111 does not show such a sudden change. This pressure range is consistent with where the deviatoric stress increased (figure 6).

Another indicator of the stress condition is the separation of ruby fluorescence lines, R_1–R_2 [24]. The positions of the fluorescence lines were determined at peak tops. The R_1–R_2 separations are shown in figure 8. The R_1–R_2 separation in Run 1 did not show significant changes below 40 GPa but became larger above this pressure. The separations in Run 2 were larger than those of Run 1 at similar pressure conditions. It is deduced that the rubies might bridge the anvils since the sample chamber of Run 2 was much smaller than that of Run 1 although we had carefully chosen and put the small rubies in to avoid the bridging between the anvils. It is not clear whether the increase of the R_1–R_2 separation at 40 GPa was due to the bridging. Considering the results shown in figure 6 with figure 8, the separation of the ruby fluorescence is probably insensitive to the uniaxial stress below approx. 0.2 GPa at least.

There are some studies to measure these stress indicators for helium and neon. The studies about the gamma plot for gold have only been carried out with a helium pressure medium (e.g. [21]). The slope of the gamma plot for gold became steeper around 30–50 GPa and the deviatoric stress was estimated from the slope [23]. About neon,

deviatoric stress measurements were carried out with x-ray diffraction [25], which reported that the stress was detectable at about 15 GPa where the value was 0.15 GPa and became larger with compression (e.g. 0.45 at 20 GPa). These values of deviatoric stress are shown in figure 6. The separation of ruby fluorescence lines in helium did not change up to 90 GPa [26], whereas deterioration of hydrostaticity in neon was found at around 20 GPa [26]. These previous results are shown in figure 8. From the comparison, the stress condition in $NeHe_2$ is most likely to between those of neon and helium. Recently, a comprehensive study about pressure distribution in the sample chamber of DAC by the ruby fluorescence measurement was published [27]. A study like that of [27] would give additional information for evaluation of $NeHe_2$ as a pressure-transmitting medium.

5. Conclusion

The hexagonal Laves-type phase of $NeHe_2$ is stable up to 90 GPa. The similarity and difference between the Laves-$NeHe_2$ and helium–neon mixture in unit cell scale and inter-atomic distances were revealed. Elasticity of the Laves-$NeHe_2$, as a macroscopic property, was similar to that of the hypothetical helium–neon mixture. On the other hand, the pressure dependence of the inter-atomic distances, as a kind of microscopic property, was different in between the Laves-$NeHe_2$ and the elementary substances. Since this material has a larger bulk modulus at low pressure conditions than neon and helium, the reduction of the sample chamber is expected to be small. Therefore, if one needs a large sample space and relatively good quasi-hydrostaticity, $NeHe_2$ can be considered an option as a pressure-transmitting medium.

Acknowledgments

We acknowledge help and advice in the experiment by Hitoshi Yusa and Nagayoshi Sata. We thank Kenichi Takemura and Satoshi Nakano for fruitful discussions and helpful comments. The constructive comments by two anonymous referees are highly appreciated. The synchrotron radiation experiments were performed with the approval of the Japan Synchrotron Radiation Research Institute (proposal no. 2008A1203). The DFT calculations were performed on the ES45 server at the Institute of Study for the Earth's Interior, Okayama University with help from Masami Kanzaki. This work was partially supported by Grants-in-Aid for Young Scientists of Japan Society for the Promotion of Science.

References

[1] Venables J A and Klein M L (ed) 1976 *Rare Gas Solids* vols I and II (New York: Academic)
[2] Rosciszewski K, Paulus B, Fulde P and Stoll H 2000 *Phys. Rev.* B **62** 5482
[3] Schwerdtfeger P, Gaston N, Krawczyk R P, Tonner R and Moyano G E 2006 *Phys. Rev.* B **73** 064112
[4] Loubeyre P, Jean-Louis M, LeToullec R and Charon-Gerard L 1993 *Phys. Rev. Lett.* **70** 178
[5] Friauf J B 1927 *Phys. Rev.* **29** 34–40
[6] Momma K and Izumi F 2008 *J. Appl. Crystallogr.* **41** 653–8
[7] Kohara S, Itou M, Suzuya K, Inamura Y, Sakurai Y, Ohishi Y and Takata M 2007 *J. Phys.: Condens. Matter* **19** 506101
[8] Fujihisa H unpublished
[9] Fei Y, Ricolleau A, Frank M, Mibe K, Shen G and Prakapenka V 2007 *Proc. Natl Acad. Sci. USA* **104** 9182–6
[10] Mao H K, Xu J and Bell P M 1986 *J. Geophys. Res.* **91** 4673–6
[11] Blaha P, Schwarz K, Madsen G, Kvasnicka D and Luitz J *WIEN2k, An Augmented Plane Wave + Local Orbitals Program for Calculating Crystal Properties* Karlheinz Schwarz, Techn. Universität Wien, Austria
[12] Anderson Y, Langreth D C and Lundqvist B I 1996 *Phys. Rev. Lett.* **76** 102
[13] Iitaka T and Ebisuzaki T 2001 *Phys. Rev.* B **65** 012103
[14] Basanta M A, Dappe Y J, Ortega J and Flores F 2005 *Europhys. Lett.* **70** 355
[15] Vinet P, Ferrante J, Rose J H and Smith J R 1987 *J. Geophys. Res.* **92** 9319–25
[16] Zha C S, Mao H K and Hemley R J 2004 *Phys. Rev.* B **70** 174107
[17] Hemley R J, Zha C S, Jephcoat A P, Mao H K, Finger L W and Cox D E 1989 *Phys. Rev.* B **39** 11820–7
[18] Dewaele A, Datchi F, Loubeyre P and Mezouar M 2008 *Phys. Rev.* B **77** 094106
[19] Loubeyre P, LeToullec R, Pinceaux J P, Mao H K, Hu J and Hemley R J 1993 *Phys. Rev. Lett.* **71** 2272–5
[20] Mao H K, Hemley R J, Wu Y, Jephcoat A P, Finger L W, Zha C S and Bassett W A 1988 *Phys. Rev. Lett.* **60** 2649–52
[21] Singh A K 1993 *J. Appl. Phys.* **73** 4278
[22] Takemura K and Singh A K 2006 *Phys. Rev.* B **73** 224119
[23] Takemura K and Dewaele A 2008 *Phys. Rev.* B **78** 104119
[24] Chai M and Brown J M 1996 *Geophys. Res. Lett.* **23** 3539
[25] Meng Y, Weidner D J and Fei Y 1993 *Geophys. Res. Lett.* **20** 1147–50
[26] Nakano S 2006 *Proc. 47th High Pressure Conf. of Japan Review of High Pressure Sci. Technol.* **16** 321
[27] Klotz S, Chervin J-C, Munsch P and Le Marchand G 2009 *J. Phys. D: Appl. Phys.* **42** 075413